

# 1 The Ekman layer model revisited

Yosef Ashkenazy,<sup>1</sup> Hezi Gildor,<sup>2</sup> Golan Bel,<sup>1</sup>

---

Corresponding author: Y. Ashkenazy, Department of Solar Energy and Environmental Physics, Blaustein Institutes for Desert Research, Ben-Gurion University of the Negev, Sede Boqer Campus 84990, Israel. (ashkena@bgu.ac.il)

<sup>1</sup>Department of Solar Energy and Environmental Physics, Blaustein Institutes for Desert Research, Ben-Gurion University of the Negev, Sede Boqer Campus 84990, Israel.

<sup>2</sup>The Fredy and Nadine Herrmann Institute of Earth Sciences, The Hebrew University of Jerusalem, Jerusalem, Israel.

2 The seminal model for the effect of winds on surface ocean currents was  
3 proposed by Ekman more than a century ago. It demonstrated the non-trivial  
4 effect of Earth's rotation on surface ocean currents driven by constant wind.  
5 Here we show that this model is ill-defined when forced by a more realistic  
6 stochastic wind—the component of the stochastic wind that resonates with  
7 the Coriolis frequency leads to the divergence of the surface and depth-integrated  
8 currents. The addition of a linear friction term to the model suppresses this  
9 unphysical divergence. We present explicit solutions for the surface and depth-  
10 integrated currents for wind stress with exponentially decaying and oscillat-  
11 ing temporal correlations and show that the wind's temporal correlations and  
12 the friction drastically affect, and can even diminish, the resonance. Winds  
13 and currents from the Gulf of Elat are compared with the model's predic-  
14 tions.

## 1. Introduction

15 Motivated by the observation of Fridtjof Nansen that ice in the Arctic drifts 20°-40°  
16 to the right of the prevailing winds, Vagn Walfrid Ekman [*Ekman*, 1905] developed, in  
17 1905, a simple model for the depth dependence of the surface current under the action  
18 of constant (or pulse-like) wind. This highly idealized model predicted a clockwise spiral  
19 rotation as a function of depth, an exponentially decaying current speed with depth, an  
20 angle of 45° of the surface current to the right of the wind, and integrated currents that  
21 are (right) perpendicular to the wind [*Gill*, 1982; *Cushman-Roisin*, 1994; *Gildor*, 2008].  
22 Ekman's model was supported by observations [e.g., *Hunkins*, 1966; *Price et al.*, 1987;  
23 *Chereskin*, 1995; *Roach et al.*, 2012] and by rotating tank experiments [e.g., *Cushman-*  
24 *Roisin*, 1994; *Vallis*, 2006; *Marshall and Plumb*, 2008]. The Ekman model is one of the  
25 most fundamental models to demonstrate the effect of Earth's rotation on the ocean  
26 currents, and basic oceanic processes (like coastal upwelling/ downwelling and Ekman  
27 transport) are based on it. However, the simplicity of the Ekman model and its simplistic  
28 assumptions (such as the constant eddy parameterized vertical viscosity coefficient) limit  
29 its applicability [*Ekman*, 1905] to the atmosphere and ocean.

30 Many studies have generalized and modified the Ekman model. Yet, only a limited  
31 number of studies have investigated the effects of stochastic wind on the surface cur-  
32 rents [e.g., *Gonella*, 1971; *McWilliams and Huckle*, 2005; *Chu*, 2009, 2008; *Ashkenazy*  
33 *and Gildor*, 2011], especially when the wind is temporally correlated [*Bel and Ashkenazy*,  
34 2013]. This is especially surprising since winds are stochastic in their nature and are far

35 from being temporally constant as was assumed by Ekman [e.g., *Seguro and Lambert,*  
36 2000; *Monahan,* 2006, 2010].

37 Here we study the Ekman layer model under the action of stochastic and temporally  
38 correlated wind stress. We demonstrate that the depth-dependent Ekman layer model  
39 is ill-defined when forced by stochastic wind stress due to the resonance of the Coriolis  
40 force (frequency) with a wind-stress component of corresponding frequency—this resonance  
41 eventually leads to the divergence of the surface currents. To avoid this divergence, we  
42 follow [*Kim et al.,* 2014] and add a linear friction term to the Ekman layer model. We  
43 present an explicit solution for the surface and depth-integrated currents. We show that  
44 the effect of the resonance strongly depends on the temporal correlations of the wind and  
45 the friction term.

## 2. Model and solution procedure

46 Based on *Ekman* [1905], we study the effect of wind stress on surface ocean currents  
47 using the following set of equations

$$u_t - fv = \nu u_{zz} - ru, \tag{1}$$

$$v_t + fu = \nu v_{zz} - rv, \tag{2}$$

48 where  $t$  and  $z$  are the time and depth coordinates,  $u$  and  $v$  are the zonal (west to east)  
49 and meridional (south to north) velocities,  $f$  is the Coriolis parameter assumed here to  
50 be constant,  $\nu$  is the eddy parameterized vertical viscosity coefficient, and  $r$  is a constant  
51 resembling Rayleigh-like friction [*Kim et al.,* 2014]. Note that the addition of the  $r$  terms  
52 is crucial for the results of this paper; they are not part of the original Ekman layer

53 model but are added here to solve the problem of the divergence of surface currents under  
 54 resonance conditions; see below.

By defining a new complex variable  $w = u + iv$ , it is possible to obtain a single equation for Eqs. (1), (2):

$$w_t + (r + if)w = \nu w_{zz}. \quad (3)$$

After applying a Fourier Transform (FT) with respect to the time variable <sup>1</sup>, we obtain the following  $z$ -dependent equation:

$$\hat{w}_{zz} - \frac{r + i(f + \omega)}{\nu} \hat{w} = 0. \quad (4)$$

We assume that the ocean is infinitely deep, that the currents vanish at depth, and that at the surface [Gill, 1982]

$$\hat{w}_z(z = 0) = \frac{1}{\rho_0 \nu} (\hat{\tau}_x + i \hat{\tau}_y) = \frac{1}{\rho_0 \nu} \hat{\tau}, \quad (5)$$

where  $\rho_0$  is the water density (assumed here to be constant), and  $\hat{\tau}_x, \hat{\tau}_y$  are the FT of the zonal and meridional wind-stress components. Under these assumptions and boundary conditions:

$$\hat{w} = \frac{\hat{\tau}}{\rho_0 \nu k} e^{kz}, \quad (6)$$

where

$$k = \frac{(r^2 + (f + \omega)^2)^{1/4}}{\sqrt{\nu}} e^{i\phi/2}; \quad \phi = \tan^{-1} \left( \frac{f + \omega}{r} \right), \quad (7)$$

such that

$$|\hat{w}|^2 = \frac{|\hat{\tau}|^2}{\rho_0^2 \nu \sqrt{r^2 + (f + \omega)^2}} e^{2(r^2 + (f + \omega)^2)^{1/4} z / \sqrt{\nu}}. \quad (8)$$

At the surface ( $z = 0$ ), Eq. (8) becomes:

$$|\hat{w}|^2 = \frac{|\hat{\tau}|^2}{\rho_0^2 \nu \sqrt{r^2 + (f + \omega)^2}}. \quad (9)$$

For the integrated currents (Ekman transport)  $\hat{W} = \int \hat{w} dz$ , we get

$$|\hat{W}|^2 = \frac{|\hat{\tau}|^2}{\rho_0^2 (r^2 + (f + \omega)^2)}. \quad (10)$$

The second moment of the currents,  $\langle |w|^2 \rangle$ , can be obtained by using the Parseval's theorem:

$$\langle |w|^2 \rangle = \frac{1}{2\pi} \int_{-\infty}^{\infty} |\hat{w}|^2 d\omega. \quad (11)$$

Thus, once the power spectrum of the wind stress,  $|\hat{\tau}|^2$ , is known, it is possible to obtain the second moment of the currents.

### 3. Temporally correlated wind stress–solution

Consider the case in which the wind stress has exponentially decaying temporal correlations superimposed on a periodic signal (representing, e.g., the diurnal cycle):

$$\langle \tau_x(\tilde{t}) \tau_x(\tilde{t} + t) \rangle = \frac{\tau_{0,x}^2}{2} e^{-\gamma_x |t|} \cos(\omega_0 t), \quad (12)$$

where  $\tau_{0,x}^2$  is a constant representing the second moment of the wind-stress in the  $x$  (zonal) direction,  $\gamma_x$  is the exponential decay rate of the temporal correlations, and  $\omega_0$  is the frequency at which the correlation function oscillates<sup>2</sup>. Here, we assume that the zonal and meridional components of the wind-stress are independent such that each component can be analyzed separately and the linearity of the model implies that the overall result is the sum of their contributions. We thus restrict ourselves below to the zonal direction where the generalization to include the meridional direction is straightforward. For simplicity,

<sup>64</sup> we drop below the subscript “x”.

The FT of Eq. (12) is

$$|\hat{\tau}|^2 = \frac{\gamma\tau_0^2}{2} \left( \frac{1}{\gamma^2 + (\omega + \omega_0)^2} + \frac{1}{\gamma^2 + (\omega - \omega_0)^2} \right). \quad (13)$$

Hence, in principle, it possible to find the second moment of the depth-dependent currents using Eqs. (8) and (11). However, it seems that there is no general analytic solution for this integral unless the wind stress is periodic and  $|\hat{\tau}|^2$  is a delta function. Yet, we find the second moment of the depth-integrated current given in Eq. (10)

$$\langle |W|^2 \rangle = \frac{\tau_0^2}{4\rho_0^2} \frac{\gamma + r}{r} \left( \frac{1}{(f + \omega_0)^2 + (\gamma + r)^2} + \frac{1}{(f - \omega_0)^2 + (\gamma + r)^2} \right). \quad (14)$$

<sup>65</sup> In the absence of periodic wind stress (i.e.,  $\omega_0 = 0$ ), this expression is consistent with our  
<sup>66</sup> previous derivations [*Bel and Ashkenazy, 2013*].

It is also possible to obtain an analytic expression for the second moment of the surface currents ( $z = 0$ ) given in Eq. (9):

$$\langle |w|^2 \rangle = \frac{\sqrt{2}}{8\pi} \frac{\tau_0^2}{\nu\rho_0^2} \sum_{j=+,-} \frac{1}{B_j} \left[ (\pi - 2\alpha_j) \sqrt{B_j + A_j} + \sqrt{B_j - A_j} \ln C_j \right], \quad (15)$$

where

$$A_{\pm} = r^2 - \gamma^2 + (f \pm \omega_0)^2 \quad (16)$$

$$B_{\pm} = \sqrt{A_{\pm}^2 + 4\gamma^2(f \pm \omega_0)^2} \quad (17)$$

$$C_{\pm} = \frac{1}{r^2} \left[ (f \pm \omega_0)^2 + B_{\pm} + \sqrt{2} |f \pm \omega_0| \sqrt{B_{\pm} + A_{\pm} + \gamma^2} + \sqrt{2}\gamma \sqrt{B_{\pm} - A_{\pm}} \right] \quad (18)$$

$$\tan \alpha_{\pm} = \frac{\sqrt{2}\gamma + \sqrt{B_{\pm} - A_{\pm}}}{\sqrt{2} |f \pm \omega_0| + \sqrt{B_{\pm} + A_{\pm}}}. \quad (19)$$

<sup>67</sup> Note that  $B_{\pm} \geq |A_{\pm}|$  such that the square roots in Eqs. (18) and (19) are always non-  
<sup>68</sup> negative.

#### 4. Limiting cases

We will consider below a few limiting cases of the general expression of the second moment of surface currents given in Eqs. (15)-(19).

**Constant wind and no friction::** In this case,  $r = 0$ ,  $\gamma = 0$ , and  $\omega_0 = 0$ . Then the second moment is  $\langle |w|^2 \rangle = \tau_0^2 / (2\nu\rho_0^2|f|)$ . This expression is consistent with the classical solution of Ekman [Gill, 1982; Cushman-Roisin, 1994; Vallis, 2006].

**Infinite friction::** In this case,  $r \rightarrow \infty$  and then  $\langle |w|^2 \rangle \rightarrow \tau_0^2 / (2\rho_0^2\nu r) \rightarrow 0$ , as expected from the very large friction.

**Zero friction::** In this case,  $r \rightarrow 0$  and

$$\langle |w|^2 \rangle \approx -\frac{\gamma \ln r}{2\pi} \frac{\tau_0^2}{\nu\rho_0^2} \left( \frac{1}{\gamma^2 + (f + \omega_0)^2} + \frac{1}{\gamma^2 + (f - \omega_0)^2} \right). \quad (20)$$

Thus the second moment diverges when  $r \rightarrow 0$ , assuming that all other parameters are finite, highlighting the problem with the traditional formulation of the Ekman layer model.

**Periodic wind::** In this case,  $\gamma \rightarrow 0$ , and when assuming a finite friction  $r$  we get

$$\langle |w|^2 \rangle = \frac{\tau_0^2}{4\nu\rho_0^2} \left( \frac{1}{\sqrt{r^2 + (f + \omega_0)^2}} + \frac{1}{\sqrt{r^2 + (f - \omega_0)^2}} \right). \quad (21)$$

When  $|f| = |\omega_0|$ , the leading order term of  $\langle |w|^2 \rangle$  varies like  $1/r$  and diverges when  $r \rightarrow 0$ . Intuitively, the latter case is equivalent to a forced harmonic oscillator without friction and under resonance conditions.

**Uncorrelated wind::** In this case,  $\gamma \rightarrow \infty$ , and when  $r > 0$ , we get  $\langle |w|^2 \rangle = [\tau_0^2 / (\pi\nu\rho_0^2)] (\ln \gamma) / \gamma \rightarrow 0$ . Thus, as expected, surface currents are not developed under the action of uncorrelated wind [see also Bel and Ashkenazy, 2013].

#### 5. Results

84 We summarize the model's results in Fig. 1. In Fig. 1a, we present the mean surface  
 85 current (in cm/s) as a function of the Coriolis and correlation parameters ( $f$  and  $\gamma$ ,  
 86 respectively). The dashed and solid lines indicate the maximal magnitude of the current  
 87 along the  $x$  ( $f$ ) and  $y$  ( $\gamma$ ) axes. For small  $\gamma$ , the maximum (resonance) occurs close to  
 88 the frequency of the wind (as  $\omega_0 = \Omega$ ), and the current is large there. However, when  $\gamma$   
 89 becomes larger, the maximum value occurs at a smaller value of the Coriolis parameter  
 90 and the maximal current is smaller; for  $\gamma/\Omega \geq 1.36$ , the maximum disappears and the  
 91 current speed decreases monotonically as a function of the Coriolis parameter,  $f$ . There  
 92 is also a maximal value as a function of the temporal correlations parameter,  $\gamma$ . A similar  
 93 optimum was reported in [Bel and Ashkenazy, 2013] for the integrated currents. There is  
 94 no maximum when the Coriolis parameter is close to the frequency of the wind ( $f \approx \omega_0$ ),  
 95 as the wind resonance with the Coriolis force overcomes the optimum due to the temporal  
 96 correlations.

97 Fig. 1b depicts the mean surface current speed as a function of the friction parameter,  
 98  $r$ , and the temporal correlation parameter,  $\gamma$ . As expected, also here there is an optimum  
 99 with respect to  $\gamma$  but not with respect to the friction parameter,  $r$ . The mean surface  
 100 current speed as a function of  $f$  and  $r$  is shown in Fig. 1c where here, as expected,  
 101 there is an optimum (resonance) with respect to the Coriolis parameter. Yet, similar to  
 102 Fig. 1a, the optimum occurs for smaller values of the Coriolis parameter as the friction,  
 103  $r$ , grows; above  $r \approx 1.2$ , there is no optimum and the surface current speed decreases  
 104 monotonically with  $f$ . Fig. 1d is similar to Fig. 1a except that here, we present the  
 105 mean current speed at a depth of 400 m. The two are qualitatively similar except that in

106 depth the currents are weaker and there is a wider range for optimal values, i.e., there is  
107 an optimal Coriolis parameter for which the  $z=-400$  m current is maximal for  $\gamma/\Omega \leq 1.7$ ,  
108 while for the surface current, there is an optimal value for  $\gamma/\Omega \leq 1.36$ . Interestingly,  
109 even at such great depths, much below the surface Ekman layer depth  $\sqrt{2\nu/\Omega} \approx 50$  m,  
110 there are noticeable currents. This is especially evident for  $\gamma \ll 1$  and  $f/\Omega \approx 1$  where the  
111 resonance is pronounced and the Ekman layer becomes very deep as  $f + \omega = 0$  [Eq. (8)].  
112 We obtained similar results to those shown in Fig. 1 when using the depth-integrated  
113 currents, using Eq. (14); the underlying mechanism of the optimum with respect to the  
114 temporal correlation parameter,  $\gamma$ , was discussed in length in [Bel and Ashkenazy, 2013],  
115 and we conjecture that a similar mechanism stands behind the results presented above.

116 We examine the predictions of the Ekman layer model described above against current  
117 measurements from the Gulf of (Aqaba) Elat, Israel. The results are presented in the  
118 supplementary material. The location of the point of measurement is  $34.92^\circ\text{E}$ ,  $29.5^\circ\text{N}$  at  
119 which the Coriolis frequency is very close to the diurnal frequency of the wind. Thus, in  
120 this location, the wind may resonate with the Coriolis force. Currents were recorded at  
121 depths of 10 m, 24 m, 36 m, and 330 m [Carlson et al., 2012, 2014]. We compare the  
122 monthly mean wind speed to the monthly mean current speed, focusing on two months,  
123 January and April 2009. The mean wind speed during April is stronger than that of  
124 January (Fig. S1a); yet, the mean current speed during January is much larger than  
125 during April (Fig. S1b,d). The resonance of the wind-forced currents with the Coriolis  
126 frequency may resolve this apparent contradiction as the winds have larger power at the  
127 diurnal band compared to the background during January 2009 (Fig. S1c).

128 To examine the effect of the resonance and to estimate the value of the friction coef-  
129 ficient,  $r$ , we have integrated Eqs. (1) and (2) using the measured winds in the Gulf of  
130 Elat; several Coriolis parameters corresponding to latitudes 20°N, 30°N, and 40°N were  
131 considered. January and April 2009 currents at different depths versus  $r$  are depicted in  
132 Fig. S2. First, it is clear that the simulated currents at 30°N are much stronger than  
133 the currents of 20°N and 40°N. Second, we estimate an upper bound for  $r$  as the crossing  
134 point of  $r$  at which the simulated mean January 2009 current becomes smaller than that  
135 of April 2009, since the observed currents are stronger than the April 2009 currents. The  
136 friction parameter corresponding to the crossing point is larger for deeper currents. Since  
137 the observations indicate that the currents during January 2009 are larger than those of  
138 April 2009, also at a depth of 10 m, and since the simulated January currents are larger  
139 than those of April only when  $r < 10^{-6} \text{ s}^{-1}$  (Fig. S2a), we conclude that  $r < 10^{-6} \text{ s}^{-1}$  for  
140 the Gulf of Elat. Alternatively, it is possible that  $r$  is depth-dependent.

141 There are several energy sources for the kinetic energy of the Gulf of Elat, including  
142 winds, tides, currents through the Straits of Tiran (the straits that connect the Red Sea  
143 with the Gulf of Elat), deep water formation, and geothermal heating [*Biton et al.*, 2008;  
144 *Biton and Gildor*, 2011a, b, 2014]. Yet, it is apparent that the winds underlie a significant  
145 part of the surface currents' kinetic energy. While the example of January versus April  
146 2009 currents provide evidence for the effect of the resonance of the Coriolis force with the  
147 wind's frequency, there are counterexamples for which the wind is strong and periodic,  
148 and yet the currents are less pronounced (e.g., June 2009, Fig. S1); in such cases, some  
149 of the other factors mentioned above may dominate the currents.

## 6. Discussion and summary

150 The seminal Ekman layer model has been used for more than a century to study the  
151 effect of winds on surface currents. Here we show that the surface currents predicted  
152 by the Ekman layer model diverge when the wind is stochastic, such that one of its  
153 components resonates with the Coriolis frequency. Many studies reported the signature  
154 of “inertial” resonance, i.e., enhanced currents as a result of resonance between the Coriolis  
155 parameter and the periodicity of the winds [e.g., *Rudnick and Weller*, 1993; *Crawford and*  
156 *Large*, 1996; *Rudnick*, 2003; *McWilliams and Huckle*, 2005; *Mickett et al.*, 2010; *Whitt*  
157 *and Thomas*, 2015] (tides can also resonate with the Coriolis frequency [e.g., *Stockwell*  
158 *et al.*, 2004]). However, the temporal correlations of the wind were largely ignored in  
159 the framework of the Ekman layer model. The temporal correlations of the wind play  
160 a significant role in the surface currents—there is an optimal correlation time for which  
161 the surface currents’ magnitude is maximal [*Bel and Ashkenazy*, 2013]. Here, we used  
162 the depth-dependent Ekman layer model to show that the temporal correlations of the  
163 winds drastically affect the currents (including the resonance of the Coriolis force with  
164 the winds) and that without a friction term added to the model, the currents diverge.

165 Although there are observations that support the predictions of the Ekman layer model  
166 [e.g., *Price et al.*, 1987; *Chereskin*, 1995; *Rudnick*, 2003], there is still a large gap between  
167 the observations and the model [e.g., *Cushman-Roisin*, 1994]. This gap may be attributed  
168 to the simplicity of the model, to the constant vertical eddy parameterized viscosity  
169 coefficient, to lateral effects, etc. It is possible that the stochastic nature of the wind

170 stress, its temporal correlations and the friction term studied here may help to better fit  
 171 observations with the predictions of the Ekman layer model.

172 **Acknowledgments.** We thank Georgy Burde and Eli Tziperman for helpful discus-  
 173 sions.

## Notes

1. The Fourier transform is defined here as  $\hat{w}(\omega) \equiv \int_{-\infty}^{\infty} w(t) e^{-i\omega t} dt$
- 174 2. When  $\tau_x = \tau_{0,x} \cos(\omega_0 t) + \tau_{1,x} \eta_t$  where  $\eta_t$  is a random variable with exponentially decaying correlations and zero mean, then  $\langle \tau_x(\tilde{t}) \tau_x(\tilde{t} + t) \rangle \approx \tau_{0,x}^2 \cos(\omega_0 t) / 2 + \tau_{1,x}^2 \langle \eta_{t+\tilde{t}} \eta_{\tilde{t}} \rangle / 2 = \tau_{0,x}^2 \cos(\omega_0 t) / 2 + \tau_{1,x}^2 e^{-\gamma_x |t|} / 2$ . This is the sum of Eq. (12) with  $\gamma_x = 0$  plus Eq. (12) with  $\omega_0 = 0$ .

## References

- 175 Ashkenazy, Y., and H. Gildor (2011), On the probability and spatial distribution of ocean  
 176 surface currents, *J. Phys. Oceanogr.*, *41*, 2295–2306.
- 177 Bel, G., and Y. Ashkenazy (2013), The relation between the statistics of open ocean  
 178 currents and the temporal correlations of the wind, *New J. Phys.*, *15*, 053,024.
- 179 Biton, E., and H. Gildor (2011a), The general circulation of the Gulf of Eilat/Aqaba  
 180 revisited: The interplay between the exchange flow through the Straits of Tiran and  
 181 surface fluxes, *J. Geophys. Res.*, *116*, C08,020.
- 182 Biton, E., and H. Gildor (2011b), Stepwise seasonal restratification and the evolution of  
 183 salinity minimum in the Gulf of Eilat/Aqaba, *J. Geophys. Res.*, *116*, C08,022.
- 184 Biton, E., and H. Gildor (2014), Energy budget of a small convectively driven marginal  
 185 sea: The Gulf of Eilat/Aqaba, *J. Phys. Oceanogr.*, *44*, 1954–1972.

- 186 Biton, E., J. Silverman, and H. Gildor (2008), Observations and modeling of pulsating  
187 density current, *Geophys. Res. Lett.*, *35*, L14,603.
- 188 Carlson, D. F., E. Fredj, H. Gildor, E. Biton, J. V. Steinbuck, S. G. Monismith, and  
189 A. Genin (2012), Observations of tidal currents in the northern Gulf of Eilat/Aqaba  
190 (Red Sea), *J. Mar. Sys.*, *102*, 14–28.
- 191 Carlson, D. F., E. Fredj, and H. Gildor (2014), The annual cycle of vertical mixing and  
192 restratification in the Northern Gulf of Eilat/Aqaba (Red Sea) based on high temporal  
193 and vertical resolution observations, *Deep Sea Res.*, *84*, 1–17.
- 194 Chereskin, T. K. (1995), Direct evidence for an Ekman balance in the California Current,  
195 *J. Geophys. Res.*, *100*(C9), 18,261–18,269.
- 196 Chu, P. C. (2008), Probability distribution function of the upper equatorial pacific current  
197 speeds, *Geophys. Res. Lett.*, *35*, L12,606.
- 198 Chu, P. C. (2009), Statistical characteristics of the global surface current speeds obtained  
199 from satellite altimetry and scatterometer data, *IEEE J. of Selected Topics in Applied*  
200 *Earth Observations and Remote Sensing*, *2*(1), 27–32.
- 201 Crawford, G. B., and W. G. Large (1996), A numerical investigation of resonant inertial  
202 response of the ocean to wind forcing, *J. Phys. Oceanogr.*, *26*, 873891.
- 203 Cushman-Roisin, B. (1994), *Introduction to geophysical fluid dynamics*, 1st ed., Prentice  
204 Hall.
- 205 Ekman, V. W. (1905), On the influence of the earths rotation in ocean-currents, *Arch.*  
206 *Math. Astron. Phys.*, *2*, 1–52.

- 207 Gildor, H. (2008), The bottom ekman layer and the apparent violation of the maximum  
208 principle, *Geophysical and Astrophysical Fluid Dynamics*, *102*(6), 593599.
- 209 Gill, A. E. (1982), *Atmosphere–ocean dynamics*, 662 pp., Academic Press, London.
- 210 Gonella, J. (1971), A local study of inertial oscillations in the up- per layers of the ocean,  
211 *Deep Sea Res.*, *18*, 775–788.
- 212 Hunkins, K. (1966), Ekman drift currents in the Arctic Ocean, *Deep Sea Res.*, *13*, 607–620.
- 213 Kim, S. Y., P. M. Kosro, and A. L. Kurapov (2014), Evaluation of directly wind-coherent  
214 near-inertial surface currents off Oregon using a statistical parameterization and ana-  
215 lytical and numerical models, *J. Geophys. Res.*, *119*(10), 6631–6654.
- 216 Marshall, J., and R. A. Plumb (2008), *Atmosphere, Ocean, and Climate Dynamics: An*  
217 *introductory text*, Elsevier Academic Press.
- 218 McWilliams, J. C., and E. Huckle (2005), Ekman layer rectification, *J. Phys. Oceanogr.*,  
219 *36*, 1646–1659.
- 220 Mickett, J. B., Y. L. Serra, M. F. Cronin, and M. H. Alford (2010), Resonant forcing of  
221 mixed layer inertial motions by atmospheric easterly waves in the northeast tropical  
222 Pacific, *J. Phys. Oceanogr.*, *40*(2), 401–416.
- 223 Monahan, A. H. (2006), The probability distribution of sea surface wind speeds. Part I:  
224 Theory and SeaWinds observations, *J. Climate*, *19*, 497–520.
- 225 Monahan, A. H. (2010), The probability distribution of sea surface wind speeds: Effects of  
226 variable surface stratification and boundary layer thickness, *J. Climate*, *23*(19), 5151–  
227 5162.

- 228 Price, J. F., R. A. Weller, and R. R. Schudlich (1987), Wind-driven ocean currents and  
229 Ekman transport, *Science*, *238*, 1534–1538.
- 230 Roach, C. J., H. E. Phillips, N. L. Bindoff, and S. R. Rintoul (2012), Anomalous ekman  
231 transport near Kerguelen island, *Proceedings of the 18th Australasian Fluid Mechanics*  
232 *Conference*.
- 233 Rudnick, D. L. (2003), Observations of momentum transfer in the upper ocean: Did  
234 Ekman get it right?, in *Near-Boundary Processes and Their Parameterization, Proceed-*  
235 *ings of the 13th 'Aha Huliko'a Hawaiian Winter Workshop*, edited by P. Müller and  
236 D. Henderson, pp. 163–170, University of Hawaii.
- 237 Rudnick, D. L., and A. Weller, R. (1993), Observations of superinertial and near-inertial  
238 wind-driven flow, *J. Phys. Oceanogr.*, *23*, 2359–2351.
- 239 Seguro, J. V., and T. W. Lambert (2000), Modern estimation of the parameters of the  
240 Weibull wind speed distribution for wind energy analysis, *J. Wind Engineering and*  
241 *Industrial Aerodynamics*, *85*, 75–84.
- 242 Stockwell, R. G., W. G. Large, and R. F. Milliff (2004), Resonant inertial oscillations in  
243 moored buoy ocean surface winds, *Tellus A*, *56*, 536547.
- 244 Vallis, G. K. (2006), *Atmospheric and Oceanic Fluid Dynamics*, 745 pp., Cambridge Uni-  
245 versity Press, Cambridge, U.K.
- 246 Whitt, D. B., and L. N. Thomas (2015), Resonant generation and energetics of wind-forced  
247 near-inertial motions in a geostrophic flow, *J. Phys. Oceanogr.*, *45*(1), 181208.

**Supporting Information: The Ekman layer model revisited**

Below we describe measurements and simulations of the currents in the Gulf of Elat, Israel.

**The Gulf of Elat:** The Gulf of Elat is a deep (down to  $\sim 2$  km), narrow ( $\sim 20$  km), and long ( $\sim 200$  km) gulf that is connected to the Red Sea through the Straits of Tiran. The currents in the gulf are mainly driven by the winds and tides. The stratification in the gulf is weak where the salinity is almost constant with time and depth ( $\sim 42$  grams of salt per kg of water), and the seasonal variations in temperature ranges between  $\sim 27^\circ\text{C}$  in the summer to  $\sim 21^\circ\text{C}$  during winter. The mixed layer depth varies between  $\sim 100$  m during summer to almost the entire water column during winter. Water exchange through the Straits of Tiran plays an important role in the circulation of the gulf. The winds in the gulf are mostly northerly.

**Measurements:** The measurements were taken at the northern tip of the gulf. The shallow depth currents were recorded using a 600 kHz Acoustic Doppler Current Profiler (ADCP) from September 10, 2008 to July 13, 2009 at  $29.4882^\circ\text{N}$   $34.926^\circ\text{E}$  (where the water depth is 400 m); the sampling interval was one hour. The deep currents (330 m) were recorded using an S4 electromagnetic current meter from October 12, 2008 to July 12, 2009 at  $29.498^\circ\text{N}$   $34.936^\circ\text{E}$  (where the water depth is 400 m), very close to the location of the ADCP; the sampling interval was 20 minutes. For more details, see [Carlson *et al.*, 2012, 2014]. Ten-minute-mean 10-m-height winds were measured at a nearby coastal deck ( $29.501084^\circ\text{N}$ ,  $34.916421^\circ\text{E}$ ).

269 **Results:** The monthly mean and standard deviation of the wind speed are depicted  
270 in Fig. S1a—it is clear that the wind was stronger and more variable during April 2009  
271 compared with January 2009. However, the monthly mean shallow depth currents (Fig.  
272 S1b) and deep currents (Fig. S1d) were much stronger in January than in April, in spite  
273 of the weaker winds during January. We attribute this enhancement of currents to the  
274 resonance of the Coriolis frequency, which is very close to the diurnal frequency at latitude  
275  $29.5^\circ\text{N}$  of the Gulf of Elat. This hypothesis is supported by Fig. S1c in which we plot  
276 the Fourier transform amplitude of the wind speed at the diurnal frequency. We first  
277 normalized the wind speed’s monthly time series by subtracting the mean and dividing  
278 by the standard deviation, to allow a comparison of the diurnal peak of the different  
279 months compared with the “noisy” background of the Fourier transform—we obtained  
280 similar shape of spectrum even without the normalization. Clearly, the January wind  
281 was more diurnally periodic than the April wind, making it more favorable to resonate  
282 with the Coriolis frequency. The temporal correlations of the wind ( $\gamma$  parameter) are not  
283 considered here as these are similar for January and April 2009<sup>1</sup>.

284 To more deeply understand the effect of the resonance with the Coriolis frequency and  
285 the effect of the friction parameter,  $r$ , on the dynamics, we numerically solved Eqs. (1)  
286 and (2), using the measured winds of Elat described above. In Fig. S2, we plot the mean  
287 current speed of January and April 2009 versus  $r$  for different depths (close to the depths  
288 of the measured currents plotted in Fig. S1) and latitudes ( $20^\circ\text{N}$ ,  $30^\circ\text{N}$ ,  $40^\circ\text{N}$ ). First,  
289 the currents at  $30^\circ\text{N}$  are much stronger than those at  $20^\circ\text{N}$  and  $40^\circ\text{N}$ , highlighting the  
290 significance of the resonance. Second, as expected, current speed decreases monotonically

291 as a function of the friction coefficient,  $r$ , and this decrease is more pronounced for the  
292 deep currents. Third, the simulated currents during January 2009 are stronger than those  
293 of April 2009 for a small enough friction coefficient. The crossing point (indicated by  
294 the vertical dashed line in Fig. S2) between simulated January and April monthly mean  
295 current speed curves (green and blue curves in Fig. S2) is larger for deeper currents. This  
296 suggests a rather small upper bound for the friction coefficient,  $r < 10^{-6} \text{ s}^{-1}$ , obtained  
297 at a depth of 10 m (Fig. S2a), since in this range, the simulated January currents are  
298 larger than the simulated April currents, as in the observations (Fig. S1b). Alternatively,  
299 Fig. S2 may indicate that  $r$  is depth-dependent.

## Notes

1. More accurately, we estimated the  $\gamma$  parameter based on the auto-correlation functions of the wind speed time series of the different months in four ways: the time-lag of the first minimal value of the auto-correlation function and at the times at which the auto-correlation function equals 0.5,  $1/e = 0.368$ , and 0.15. In two measures the  $\gamma$  value of January 2009 was larger than that of April 2009, disabling confident estimation of the value of  $\gamma$ .

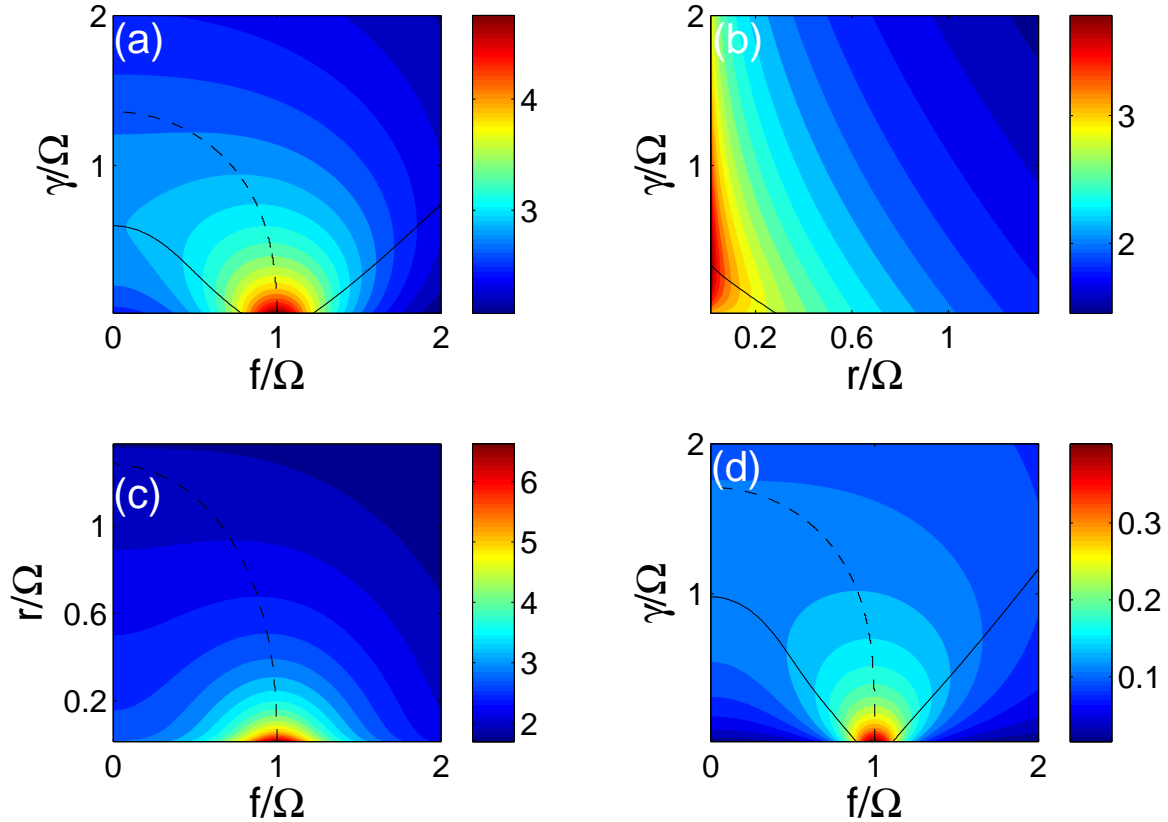


**Figure 1.** (a) Mean surface current speed (in cm/s) as a function of the Coriolis parameter (frequency),  $f$ , and the temporal correlation parameter,  $\gamma$ . (b) Same as (a) but for the friction parameter  $r$  and temporal correlation parameter  $\gamma$ . (c) Same as (a) but for the friction parameter  $r$  and the Coriolis parameter  $f$ . (d) Same as (a) but for the current at a depth of 400 m. In all panels, the solid line indicates the maximum value along the vertical axis while the dashed line indicates the maximum value along the horizontal axis. Parameter values are:  $\Omega = 2\pi/86400 \text{ s}^{-1}$ ,  $f = 2\Omega \sin(45^\circ)$ ,  $\omega_0 = \Omega$ ,  $\tau_0 = 0.1 \text{ N m}^{-2}$ ,  $\nu = 0.1 \text{ m}^2 \text{ s}^{-1}$ ,  $\rho_0 = 1028 \text{ kg m}^{-3}$ ,  $r = 10^{-5} \text{ s}^{-1}$ ,  $\gamma = 10^{-5} \text{ s}^{-1}$ .

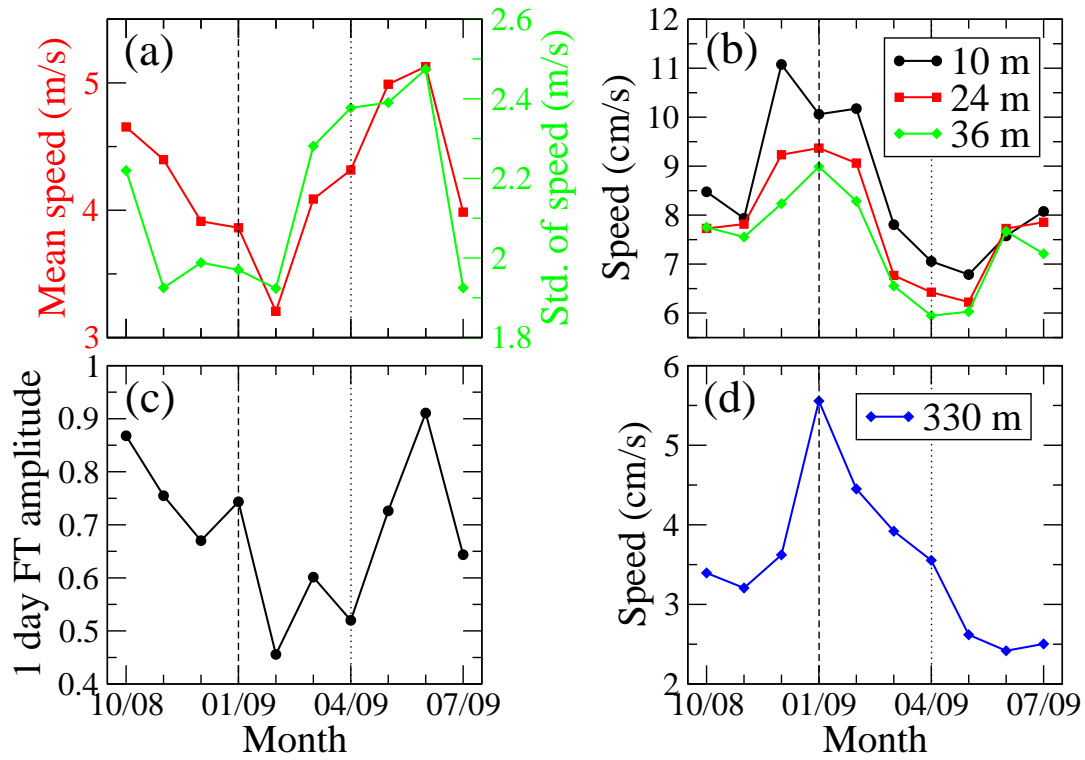


**Figure S1.** (a) Monthly mean (red) and standard deviation of the wind speed (in m/s) from the Gulf of Elat ( $34.92^{\circ}\text{E}$ ,  $29.5^{\circ}\text{N}$ ). (b) Monthly mean current speed (in cm/s) at different shallow depths. (c) FT amplitude of the wind speed at the diurnal frequency. (d) Monthly mean current speed (in cm/s) at a depth of 330 m. The vertical dashed line indicates January 2009 and the vertical dotted line indicates April 2009.

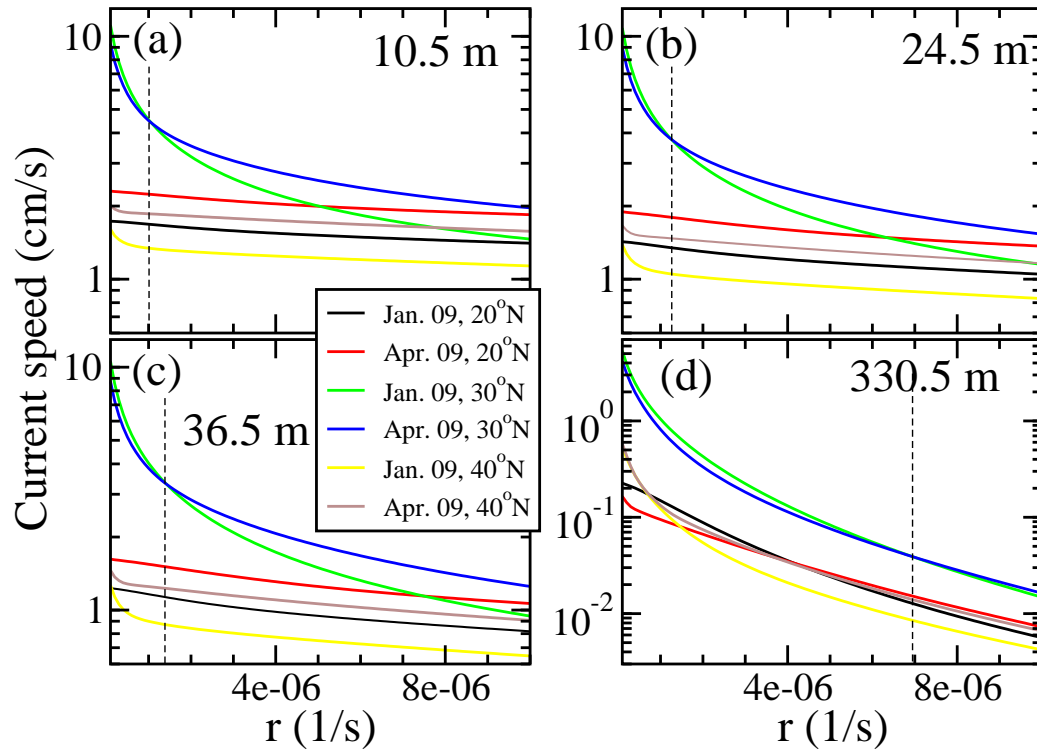


**Figure S2.** Mean simulated current speed as a function of the friction coefficient,  $r$ , when forced by the observed winds of January and April 2009 from the Gulf of Elat, for different latitudes (20°N, 30°N, and 40°N) and depths: (a) 10.5 m, (b) 24.5 m, (c) 36.5, and (d) 330.5 m. The vertical dashed line indicates the transition point at which the mean current speed of January 2009 becomes smaller than that of April 2009.